Final Report
DURIP AFOSR Grant FA9550-06-1-0285
May 1, 2006-April 15, 2007
Advanced Laser and RF Plasma Sources and Diagnostics
J. E. Scharer, PI
Electrical and Computer Engineering Department
Center for Plasma Theory and Computation
University of Wisconsin – Madison

Abstract

We have purchased and have running state-of-the-art equipment that enhances our research capabilities for efficient laser initiation and radiofrequency sustainment of plasmas and diagnostics in air, as well as near microwave windows and on cathode surfaces as part of the MURI on Nano-physics of Electron Emission and Breakdown for High Power Microwaves. Our current research on AFOSR Grant FA9550-06-1-0172 is greatly enhanced by the new source equipment and diagnostics. We have purchased equipment that will enable experimental demonstration of an instantaneous and highly efficient (> 90%) matching scheme for a pulsed high-density (10^{12-13}/cc), large-volume (>500 cc) laser-initiated and rf-sustained high-pressure plasma source. We have also purchased and have operative optical, vacuum chamber and diagnostic equipment for UV laser formation of microplasmas in air (70 Torr to 5 atm) as well as near a dielectric window to examine microwave breakdown processes. Our 200 mJ, 20 ns pulse time, 10 MW, 193 nm wavelength UV excimer laser can now produce focused power fluxes of $S=10^{8-11}$ W/cm^2 that are comparable to and can exceed current high power microwave power breakdown fluxes. Research literature has shown that microwave, laser, and radiofrequency air breakdown are all caused by an electron cascade process that lies on a <u>universal</u> breakdown field vs. pressure curve that makes the laser breakdown relevant to the microwave window breakdown process. We also have purchased an ACTON spectrometer (0.75 m focal length) with Princeton ICCD detector and camera to measure the optical emission and shadowgraphy from the window breakdown process. This diagnostic will provide high resolution (0.03 nm) spectral measurements for density and temperature diagnostics for both our laser window and radiofrequency air plasmas. We have also acquired a tunable 668 nm diode laser, optical filters, splitters, wavemeter, isolators, a fast scope and lock-in amplifiers to carry out laser-induced fluorescence (LIF) to measure rf plasma source ion drifts and temperature distributions for our laser and RF formed plasmas. This equipment has been made operative and we can now measure plasma Doppler ion drift and temperatures non-invasively that correspond to 0.1 picometer = 0.0001 nm wavelength resolution or 0.001 eV accuracy. This new equipment is allowing us to make substantial advances in efficient production and diagnosis of instantaneous, high-density, pulsed plasma production, and the nanophysics of high-power microwave window breakdown. The following sections describe the new plasma source systems and state-of-the-art diagnostics we have developed with this equipment in 1) laser-RF formed high density plasmas, 2) laser focus air breakdown and comparison with microwave breakdown and 3) measurement of plasma ion distributions in plasma sources. The report concludes with a detailed list of the equipment purchased and prices.

Table of Contents

I. High-Pressure Laser-RF Plasma Experiment Equipment Upgrade (Siqi Luo, Ryan Giar and John E. Scharer)

The overall schematic diagram of the high-pressure laser-RF plasma experiment at the University of Wisconsin–Madison is presented in Fig. 1. The objective of this experiment is to study the laser-initiated, RF-sustained plasma in the atmospheric pressure region (760 Torr). The new DURIP equipment includes the matching network updated with RF detecting and dynamic tuning system and the Spectrograph and ICCD imaging system. The 105 GHz millimeter wave interferometer is also updated with a new I-Q mixer. The updated equipment is presented in Fig. 1 in blue color. This experiment shares the key equipment, a Lumonics Pulsemaster excimer laser, with the new laser focused air breakdown plasma experiment. So an effective arrangement is made in which the laser focused air breakdown system is inserted between the excimer laser and the high-pressure laser-RF plasma system (Fig. 2). In this arrangement, two experiments can be carried out simultaneously with minimal interference. The above mentioned new and updated equipment have allowed us to advance the high pressure laser-RF plasma experiment as will be shown in the next two sections.
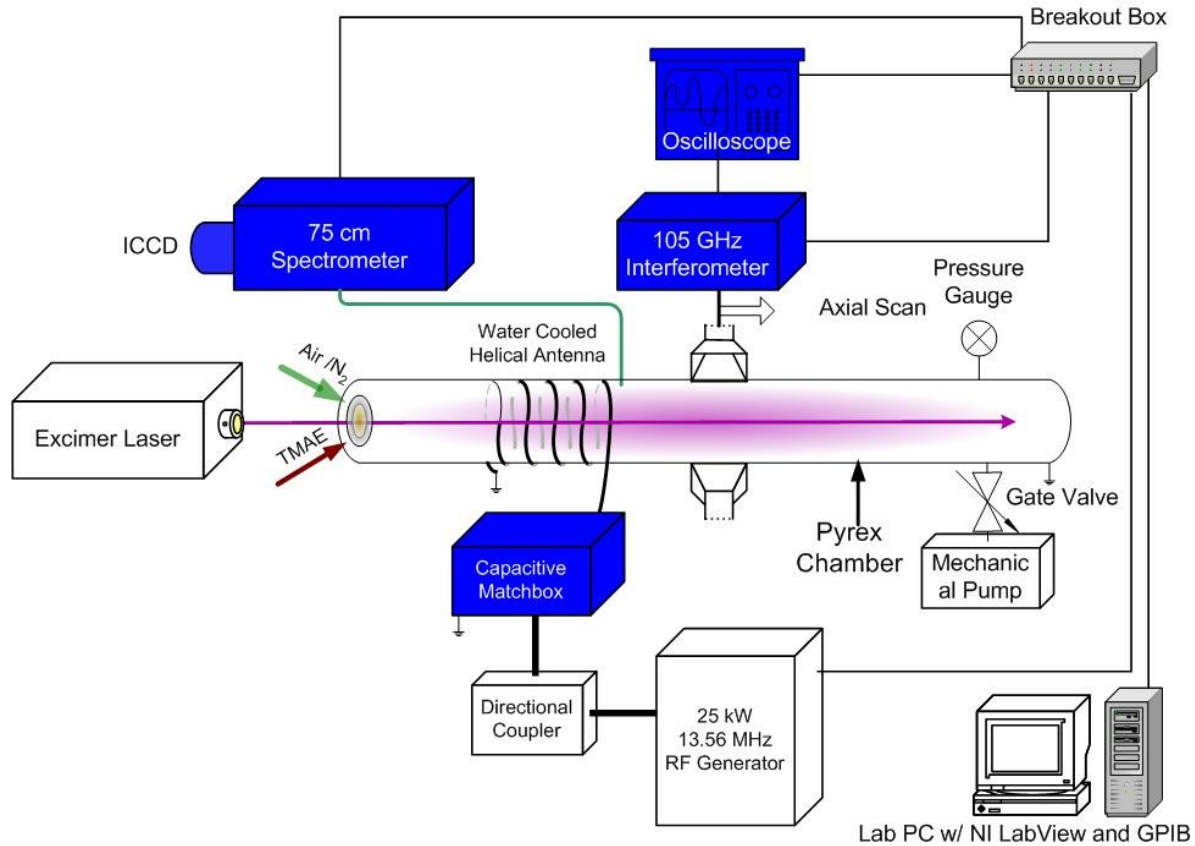

Fig. 1: Schematic diagram of the high pressure Laser-RF plasma experiment.

Fig. 2: Photograph of the high-pressure plasma arrangement. Both the laser focused air breakdown system and the high pressure laser-RF plasma system are aligned with the excimer laser so the two experiments can be carried out in tandem.
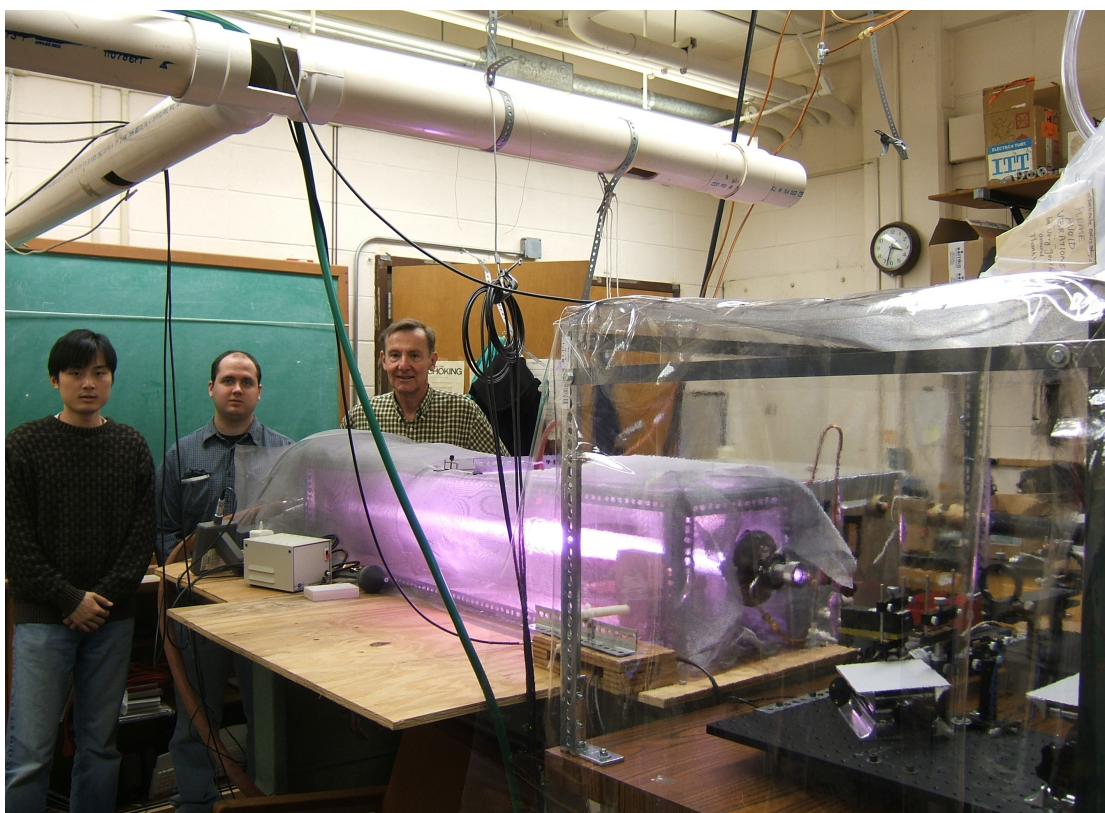

Fig. 3. Laser-RF Plasma System (Siqi Luo, Ryan Giar and John Scharer)

I.A. New RF Detecting and Dynamic Tuning System

The RF detecting circuit employs a dual directional coupler, a set of RF envelope detectors, and a comparator circuit to detect and compare the incident and reflected RF power at the input of the match box (Fig. 4). The dynamic tuning system, also show in Fig. 4, is composed of a set of high voltage RF relays that switch the matching circuit timed with the comparator output signal. This RF detecting and dynamic tuning system enables fast plasma generation within 0.5 seconds in 760 Torr air and nitrogen, and ensures low RF power reflection during the entire plasma pulse (Fig. 5). The high pressure air plasma thus created is shown in Fig. 6.
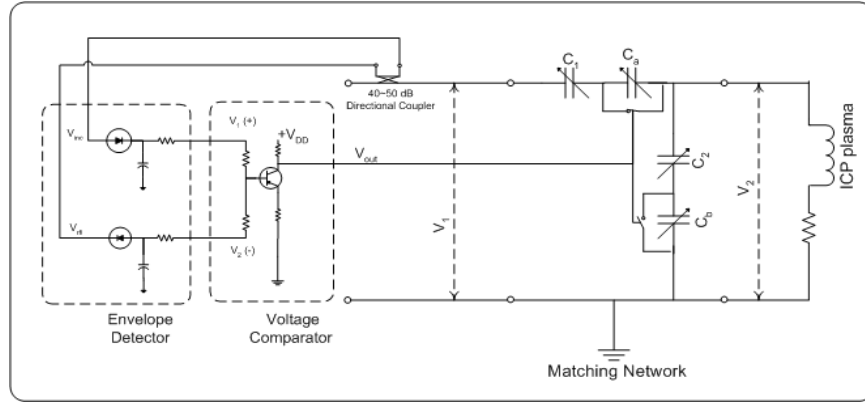

Fig. 4: Circuit diagram of the RF power matching system including the RF power detecting and dynamic tuning circuit.
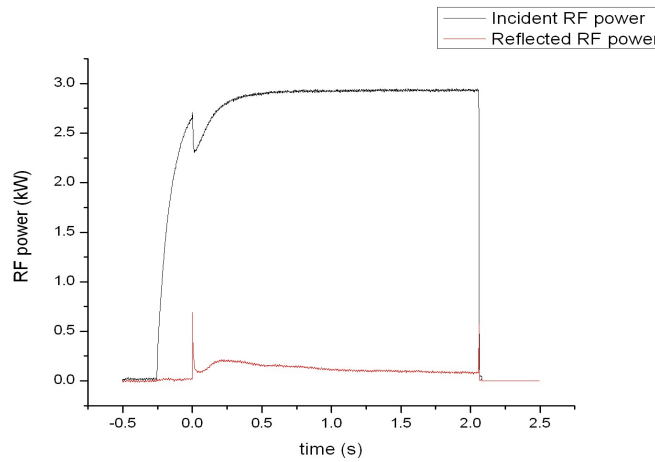

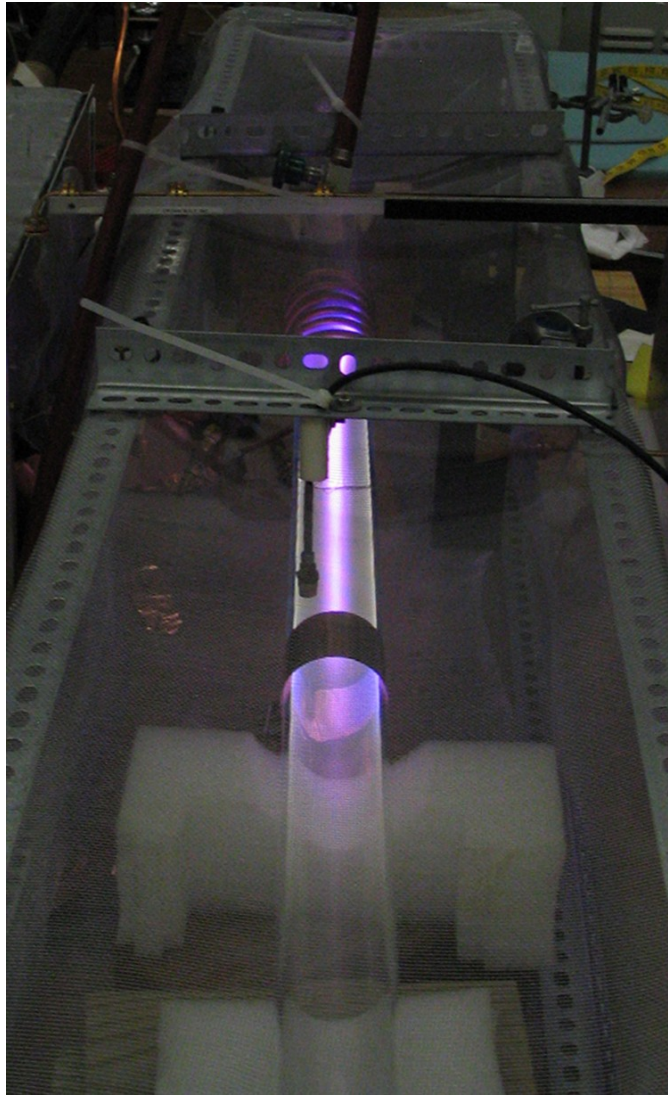Fig. 5: Incident and reflected RF power during a 2-second plasma pulse.

Fig. 6: Photograph of the high-pressure air plasma.

I.B. New Spectrograph and ICCD imaging system

The new Acton 0.75 m spectrograph and Andor ICCD equipment allows us to accurately diagnose the high-pressure air plasma optical emission spectroscopy, and infer thermodynamic characteristics of the plasmas created, especially the rotational and vibrational temperatures of certain plasma species (T_{rot} and T_{vib}), such as N_2. Because the profiles of the molecular transitions such as N_2 C-B are a strong function of the rotational and vibrational temperatures, we can infer these temperatures by matching the experimental spectra to the computer simulated ones and finding the best matching temperatures (Fig. 7).
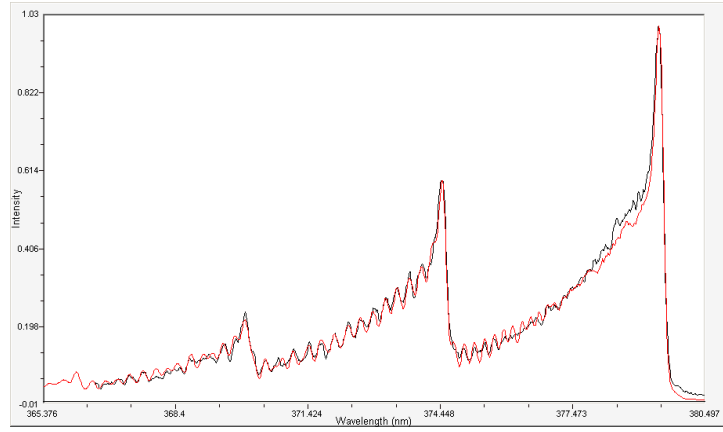
Fig. 7: Match between the experimental and computational N_2 C-B spectra. T_{rot}=1800 K, T_{vib}=2400 K is inferred from the best fit.

Optical emission spectra are taken at a series of lateral positions along the radius of the plasma column. The lateral emission signals are then Abel-inverted into radial emission signals. A special air plasma spectra simulation program, Specair, is used to simulate the emission spectra based on parameters including T_{rot} and T_{vib}. The best fit temperatures are good indications of actual temperatures in the plasmas created. Furthermore, the radial variation of T_{rot} and T_{vib} can be obtained by fitting simulated spectra to actual spectra from different radial positions. The results are presented in Fig. 8.
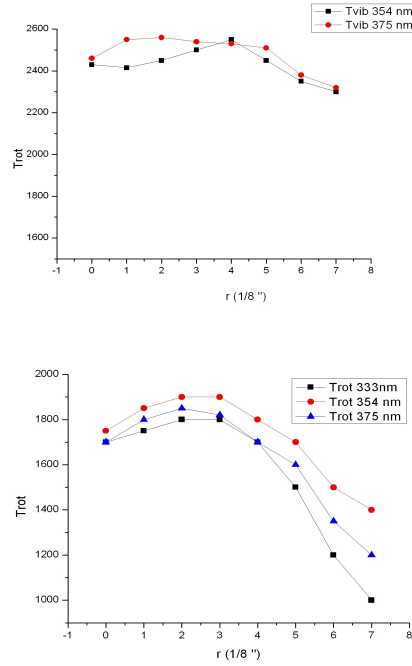

Fig. 8: Rotational and vibrational temperatures of N_2 from the N_2 C-B radiation.

II.   New Laser Focused Air Breakdown Plasma System (Magesh Thiyagarajan and John E. Scharer)

The completely new, DURIP funded experimental setup for the 193 nm laser focused electrical breakdown is shown as a schematic diagram in Fig. 9. The objective is to study air plasma breakdown in the range of 90 to 760 Torr air and use laser-to-microwave frequency scaling to relate to the MURI microwave breakdown conditions. The experimental setup utilizes our existing 193 nm UV excimer laser and the new experimental equipment is shown in blue on Fig. 9. A uniform intensity ultraviolet (UV) beam of 193 nm wavelength is produced using the excimer laser (Lumonics Pulsemaster PM-842) that runs in the ArF (6.4 eV per photon) mode.
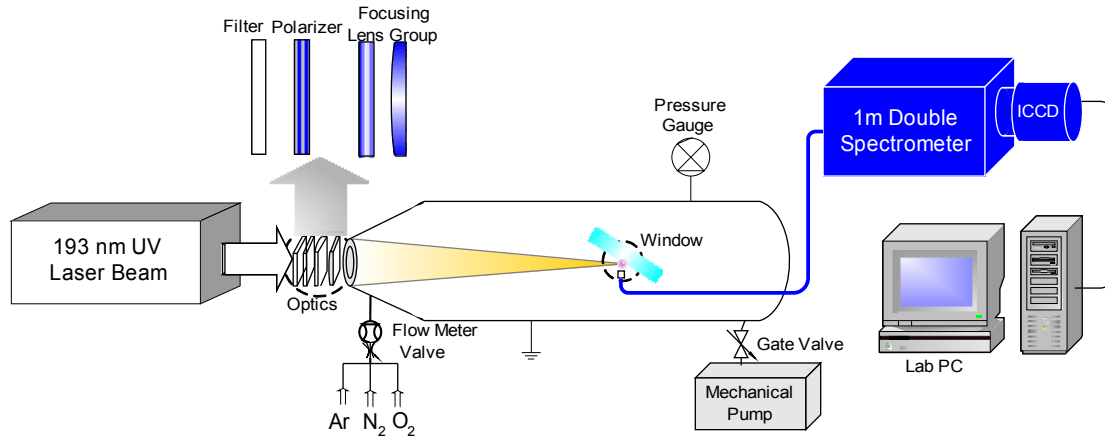

Fig. 9: Experimental setup for focused laser breakdown.

The laser beam passes through a 193nm UV optics group, which consists of a polarizer for parallel or perpendicular polarization of the laser beam, a 6 cm diameter and 15 cm focal length lens with an anti reflection coating, and a 5 cm diameter fused silica window. These are special optics designed to work with 99% transparency at 193 nm. The chamber pressure is varied in the range of 90 Torr to 760 Torr using a mechanical pump and the pressure is monitored accurately using a MEMS-based pressure gauge (MKS model 910). For background gas dry air will be our major interest. The system also has three primary diagnostic systems: shadowgraphy diagnostics to investigate the spatial and temporal evolution of the breakdown and plasma expansion, two-color interferometry technique for electron and neutral number density measurements, and optical emission spectroscopy diagnostics for density and temperature measurements.

II.A.   Temporal and Spatial Evolution Measurements Using Optical Shadowgraphy Technique
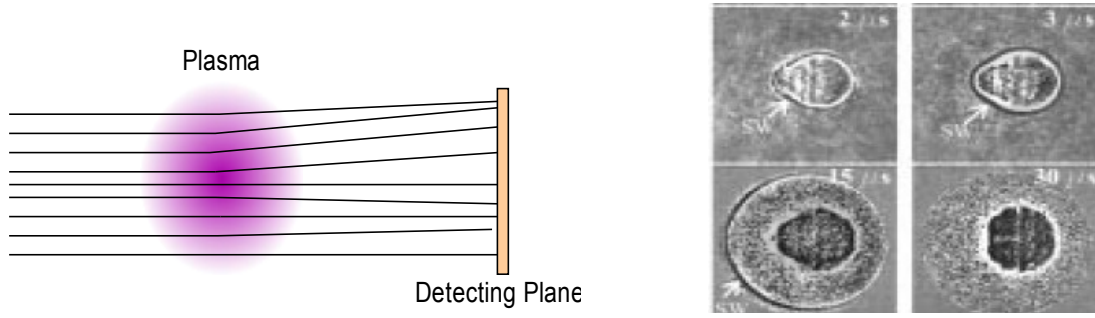

Fig. 10: (a) Refraction of a laser beam by a nonuniform plasma. (b) Shadowgraphic image of a laser induced plasma evolution

An optical shadowgraphy technique is used for temporal and spatial evolution of the plasma. In this technique a beam of light from an intense source, usually a low power (5 – 10 mW) probe laser, is launched through the plasma and falls directly upon a photographic detecting plane as shown in the Fig. 10.(a). If the refractive index in the test section n is uniform, the screen will be essentially uniformly illuminated. If, however, the gradient of n varies in space, as one may expect in high density $(10^{14} – 10^{18}$ cm$^{-3})$ plasma, - i.e., if there is a second derivative of the refractive index – there will be variations in the illumination of the screen as shown in the Fig. 10 (b). For example, regions where the second derivative is negative will act like converging lenses. The spatial variation of the refractive index across a probing beam is measured by shadowgraphy to give information on the plasma.

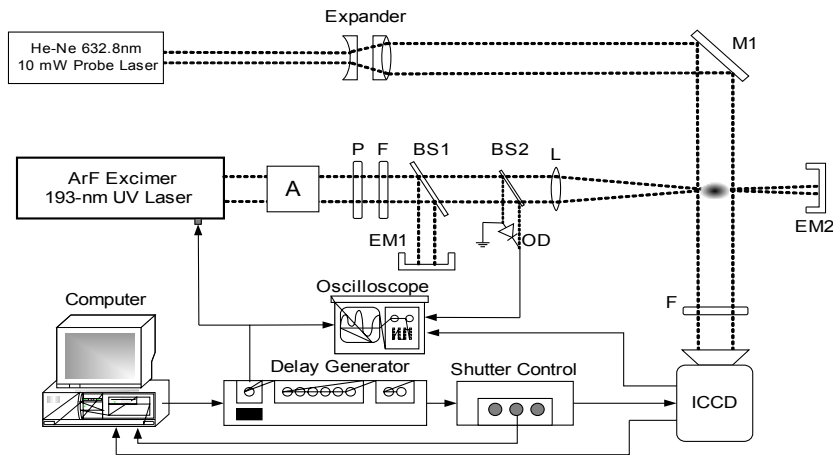## II.A.1.   New Shadowgraphy Diagnostic Setup

Fig. 11: Schematic of the shadowgraphy technique. Attenuator (A), Polarizer (P), Filter (F), Beam Splitter (BS), Lens (L), Mirror(M).

The schematic diagram of the shadowgraphy diagnostic setup is shown in Fig. 11. In this setup a He-Ne laser at $\lambda = 632.8$ nm (JDS Uniphase, model 1125P) operating in the TEM$_{00}$ mode with a power of 10 mW and beam diameter of 0.81 mm will be used as the probe laser. The laser beam is expanded 20 times to cover the entire plasma area ($\sim$1-2 cm^2) using an optical expander. The beam is operated in

the CW mode and sent through the plasma falling directly onto the Intensified CCD (Fig. 12).

Fig. 12: New Gen III ICCD detector

The imaging operation is synchronized with the laser breakdown using a delay generator and shutter control. The optics setup is positioned rigidly on a very stable workbench in order to overcome any small vibrations.

II.B. Plasma Electron and Neutral Density Measurements Using Two-Color Optical Interferometry Technique

II.B.1. Optical Interferometry

Optical interferometry is a non-perturbing diagnostic technique used to measure plasma density. Microwave interferometry is limited in range of application due to plasma frequency cutoff. Laser induced plasma densities range from $10^{15} - 10^{20}$ cm^{-3}, which demand optical interferometry diagnostics. This technique is based on the spatial variation of the refractive index, similar to the shadowgraphy technique.
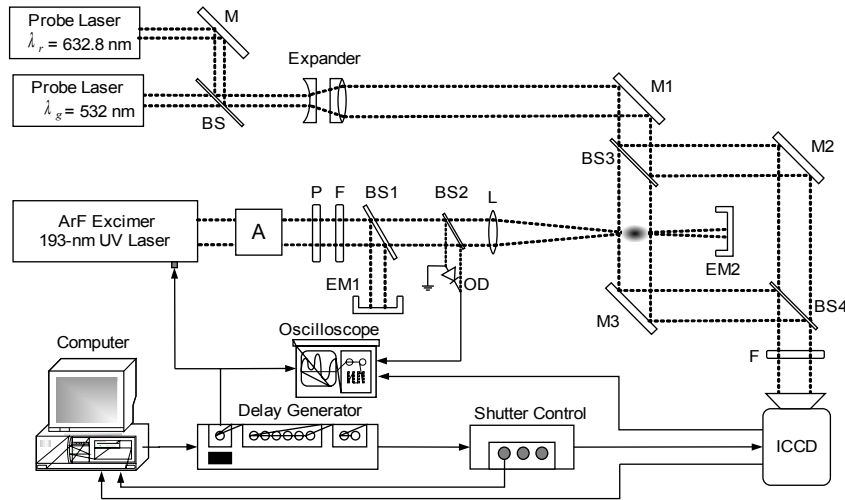

Fig. 13: Experimental setup of the two-color interferometry plasma and neutral density measurements.
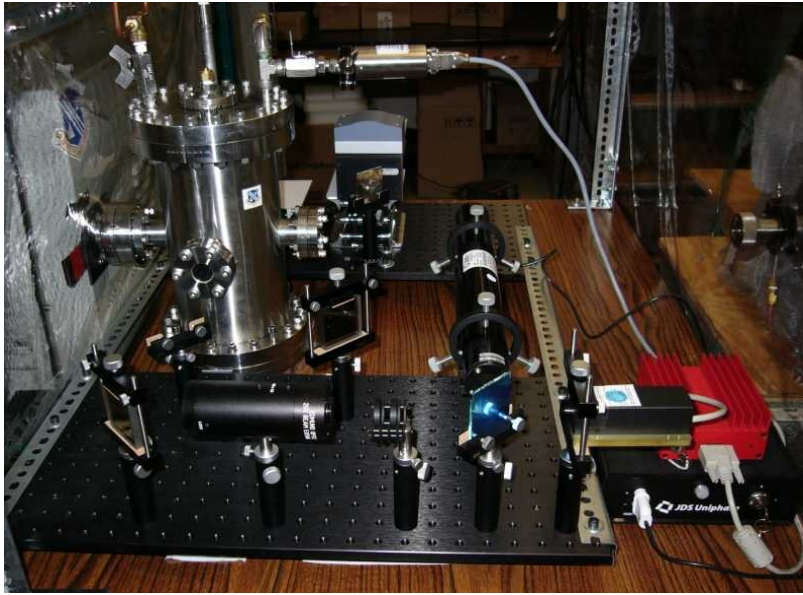
Fig. 14: New laser focus vacuum chamber and laser interferometer optical systems.

In this setup the plasma is situated in one arm of the Mach-Zender interferometer, which is illuminated with a 20X expanded beam from two lasers as shown in Fig. 13 and 14. The first one is a red He-Ne laser emitting at $\lambda = 632.8$ nm (JDS Uniphase) and the second one is a green solid-state laser at $\lambda = 532$ nm with powers of 5 and 10 mW, respectively. The probe beams will be sent one at a time to the Intensified CCD (ICCD). The camera is synchronized with the 193 nm UV pulsed laser using a delay generator. A time variable trigger pulse can be set to acquire data at different time steps. Each snap shot of the plasma fringes can yield a complete spatial profile of the plasma and multiple plasma fringes can be obtained at any time step using the ICCD controlled triggering. The plasma fringe image data is obtained, and each fringe is generally line integrated. Therefore the Abel inversion technique can be used to convert the line-integrated data to localized values.

II.C.   Temperature Measurements Using Optical Emission Spectroscopy (OES)

II.C.1.   Temperature Measurements in Local Thermodynamic Equilibrium

The temperature at early stages of the breakdown spark development will be obtained from the relative intensities of O-II lines as described by Griem. The laser induced plasmas are generally observed to be in Local Thermodynamic Equilibrium (LTE) since these laser induced plasmas are at high density (10^{16}-10^{20} cm^{-3}) and high temperatures ($1 - 5$ eV). For plasmas in LTE, a single temperature characterizes all internal energy modes (excitation, vibrational and rotational). This temperature can be determined from the absolute intensity of any atomic or molecular feature, or from Boltzmann plots of vibrational or rotational population distributions. For a pure nitrogen plasma the band of N_2 second positive system ($C^3\pi_u \rightarrow B^3\pi_g$) N_2(2+) will be used to measure the electron temperature. The second positive band system of N_2 (C-B) and atomic lines of O and N appear at higher temperatures ($\sim >1$ eV). The spectral simulations will be done with the SPECAIR code developed by Laux *et. al.*, The current version of SPECAIR models 37 molecular transitions of NO, N_2, N_2^+, O_2, CN, OH, NH, C_2, and CO, as well as atomic lines of N, O, and C. The model provides accurate simulations of the absolute spectral emission and absorption of air from 80 nm to 5.5 µm.
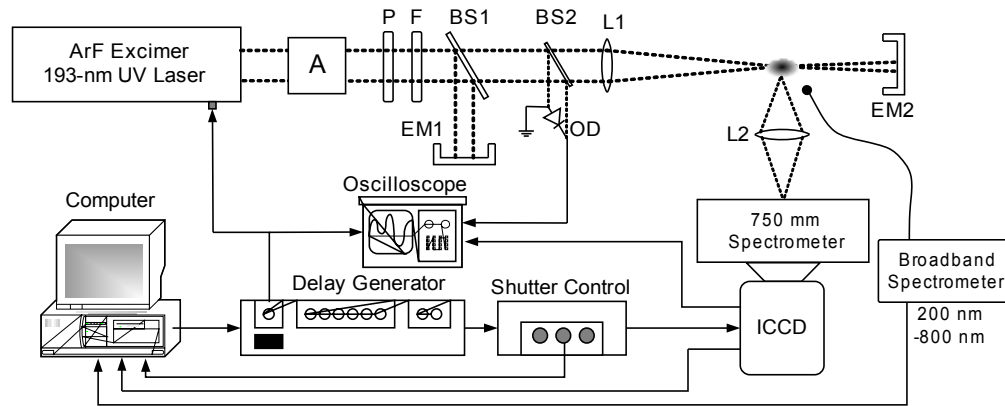
II.C.2. Spectroscopic Measurement Setup

Fig. 15: The experimental setup for temperature measurements by optical emission spectroscopy.

The optical emission spectroscopy diagnostic setup is shown in the Fig. 15. This setup will be used to measure the plasma temperature at the beginning stages of the air breakdown plasma.

Fig. 16: The spectroscopy system: monochromator (Acton Research, Model: ARC-SP-2758) and ICCD (Andor iStar, see Fig. 12).

We will use our new, DURIP funded, high resolution (0.03 nm resolution) spectroscopy system which is composed of a monochromator (Acton Research, Model: ARC-SP-2758) and an ICCD (Andor iStar) (Fig. 16). Our new ICCD is a high-performance, intensified imaging system with a high-resolution (30 μm) filmless generation-III intensifier, which provides highest sensitivity (Quantum Efficiency) from the blue (300 nm) to NIR (800 nm) wavelengths. This provides us a wide range of spectral analysis throughout the visible region with good quantum efficiency. The ICCD has a large imaging array of 1024 x 1024 pixels (13 x 13 μm) with 1:1 aspect ratio, with a pixel resolution of 30 μm. Although the monochromator continues to receive the plasma emission throughout the breakdown process, we can acquire emission within a narrow range (μs) time exposure of the ICCD by preprogrammed triggering with a variable time delay. By doing so the temperatures at different times

of the plasma breakdown process and be analyzed.

III.   Helicon System Description (C. Mark Denning, Matt Wiebold and John E. Scharer)

DURIP-funded equipment has greatly improved the diagnostic capabilities on the Helicon Plasma Experiment. The objective of the experiment is to investigate high-efficiency plasma production and the basic plasma physics of double-layer and particle transport in helicon plasmas. Graduate students Mark Denning and Matt Wiebold conduct research in the lab with John Scharer as advisor. The experiment consists of a vacuum chamber with radio frequency antenna and generator sources and associated diagnostics. The chamber consists of a 150 cm long, 10 cm inner diameter Pyrex tube connected to a 60 cm long, 45 cm inner diameter stainless steel expansion chamber, which is a recent DURIP-funded addition. Two Varian (550 L/s) turbo pumps, one at the gas inlet side and one connected to the downstream expansion chamber provide differential pumping and base pressures as low as 10^{-6} Torr. A copper half-turn double-helix antenna wrapped around the Pyrex tube couples up to 3 kW of 13.56 MHz RF power for plasma production. Typically argon plasma is generated, with pressures ranging from 0.1 mTorr to 10 mTorr. Two RF generators are available, a 1 kW pulsed unit and a 3 kW CW unit. A matchbox consisting of two high-voltage variable capacitors enables an excellent match to the plasma antenna impedance and operation with almost no power reflection to the RF generator. A static axial magnetic field is generated with seven electromagnets spaced to produce a non-uniform magnetic nozzle at the entrance to the expansion chamber, up to 200 A of current can be supplied to produce field peaks up to 1.5 kG and plasma source region fields up to 1 kG.
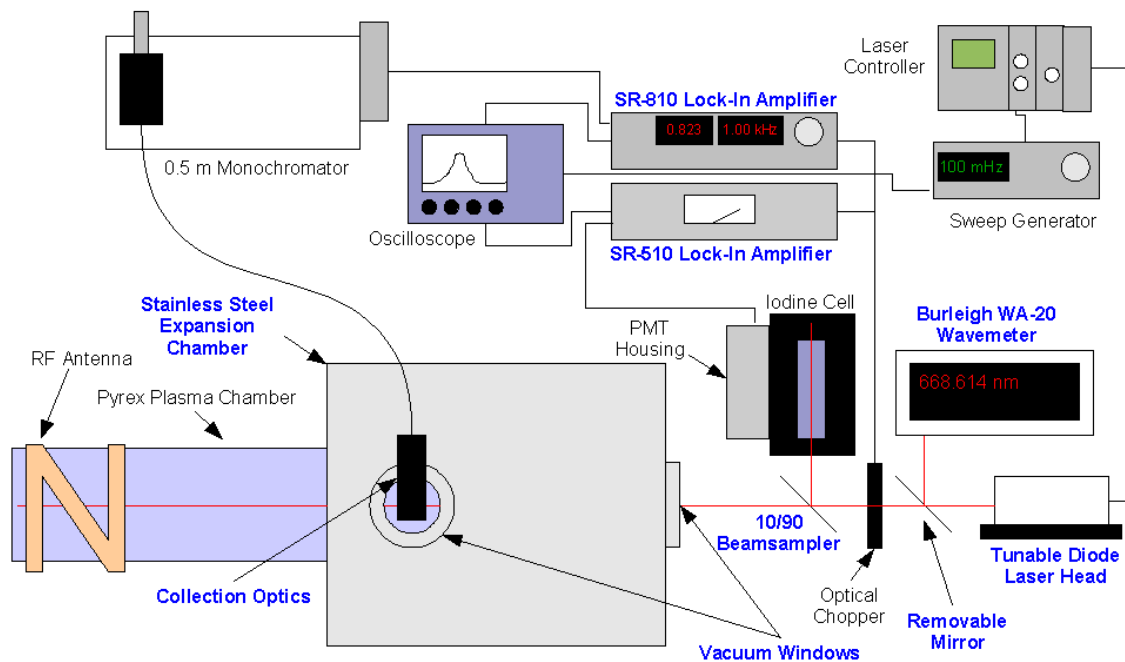

Figure 17: Laser-induced fluorescence diagnostic (DURIP-funded additions have blue captions)

Diagnostics available include current collecting and wave magnetic field probes, microwave interferometry, and laser-induced fluorescence. The new, state-of-the-art laser-induced fluorescence (LIF) diagnostic consists of a Sacher Lasertechnik 668 nm tunable diode laser in Littrow configuration. LIF is used to accurately measure the velocity distribution function of ions in the plasma to determine the drift velocity and temperature. The beam wavelength is determined using a DURIP-funded Burleigh WA-20 wavemeter (0.001 nm resolution) and is further monitored by detecting iodine cell

fluorescence with a photomultiplier tube, allowing for determination of the laser wavelength with an extremely precise resolution of 0.0001 nm. A 45º mirror reflects light onto a 10 cm focal length plano-convex lens delivering the light to a fiber collimator and ultimately to a 0.5 m focal length monochromator with PMT detector. The beam is optically chopped at 1 kHz allowing two Standford Research Systems lock-in amplifiers (DURIP-funded) to extract the signal from background noise for both the iodine cell and plasma fluorescence PMT detectors. A variety of probe diagnostics are available including a cylindrical Langmuir probe for determination of plasma density and electron temperature. An emissive probe consisting of a biased, heated filament is used to determine the spatial variation of the plasma potential along the axis of the experiment. A Mach probe which uses two collecting electrodes separated by a ceramic dielectric is also available to determine plasma drift velocity. A wave magnetic field probe consisting of a small (2 mm diameter) glass-shielded 5-turn coil is used to characterize helicon wave propagation in the plasma.105 GHz microwave interferometry is also used to determine plasma density.
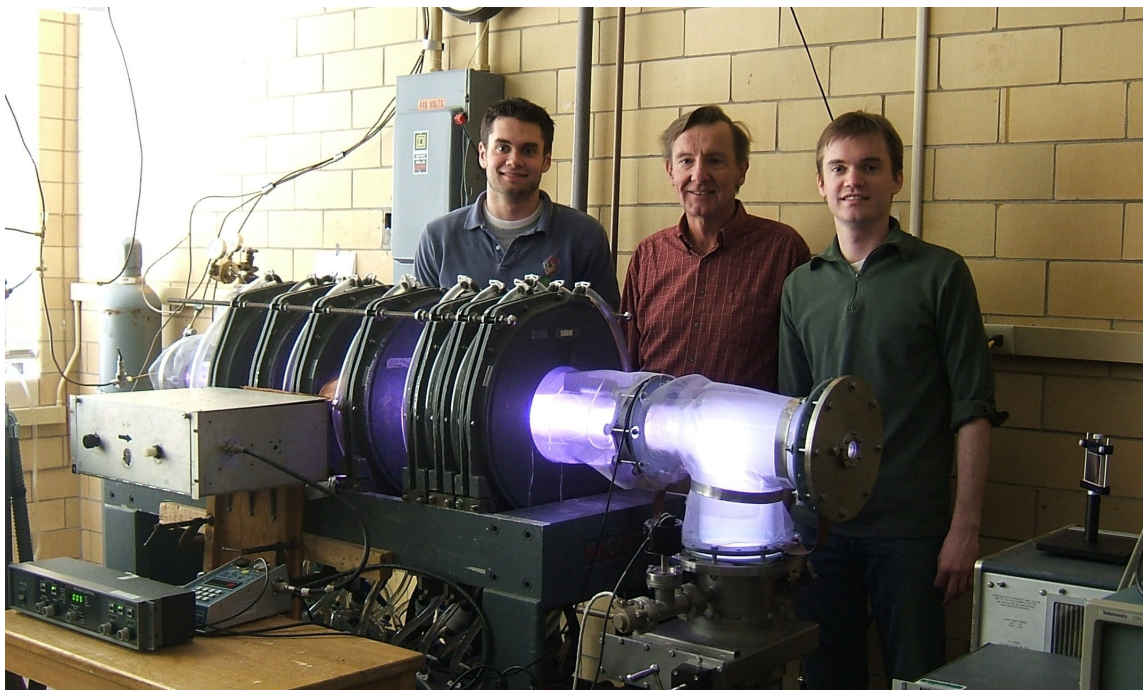

Fig. 18: Photo of the helicon plasma in operation. (Left to right) Matt Wiebold, John Scharer, and Mark Denning.
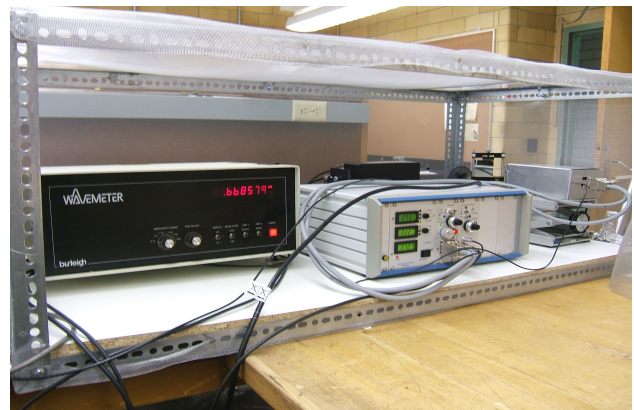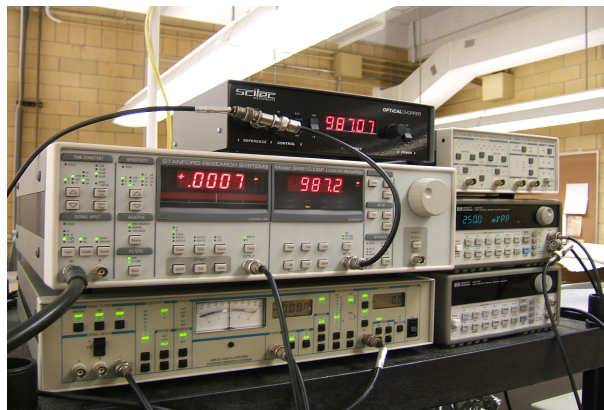

Fig. 19: Left: Lock-in amplifiers, chopper controller, and sweep generator. Right: Wavemeter, laser head and controller, and iodine cell.

Preliminary results have been obtained on the argon laser-induced fluorescence diagnostic. The wavelength of the laser is tuned over a narrow bandwidth (~8 Mhz) by varying the laser cavity size with a piezo transducer. The rough laser wavelength is determined using the Burleigh WA-20 Wavemeter and is further monitored by detecting fluorescence of iodine vapor by passing a portion of the laser beam through an iodine reference cell. Since the iodine lines in the vicinity of the laser central wavelength are known they enable measurement of the laser wavelength with 0.0001 nm accuracy. Figure 20 shows recent results obtained by the diagnostic. The dotted red line is the iodine fluorescence spectrum and the solid blue curve is the signal detected by the monochromator photomultiplier tube after lock-in amplification to reject the significant background optical emission. Curve fitting indicates that the temperature of the ions is roughly 0.06 eV. The vertical blue line indicates the laser frequency at which the argon excitation occurs. The LIF signal is Doppler down-shifted slightly from this frequency, indicating a small flow (300 m/s) away from the laser source.
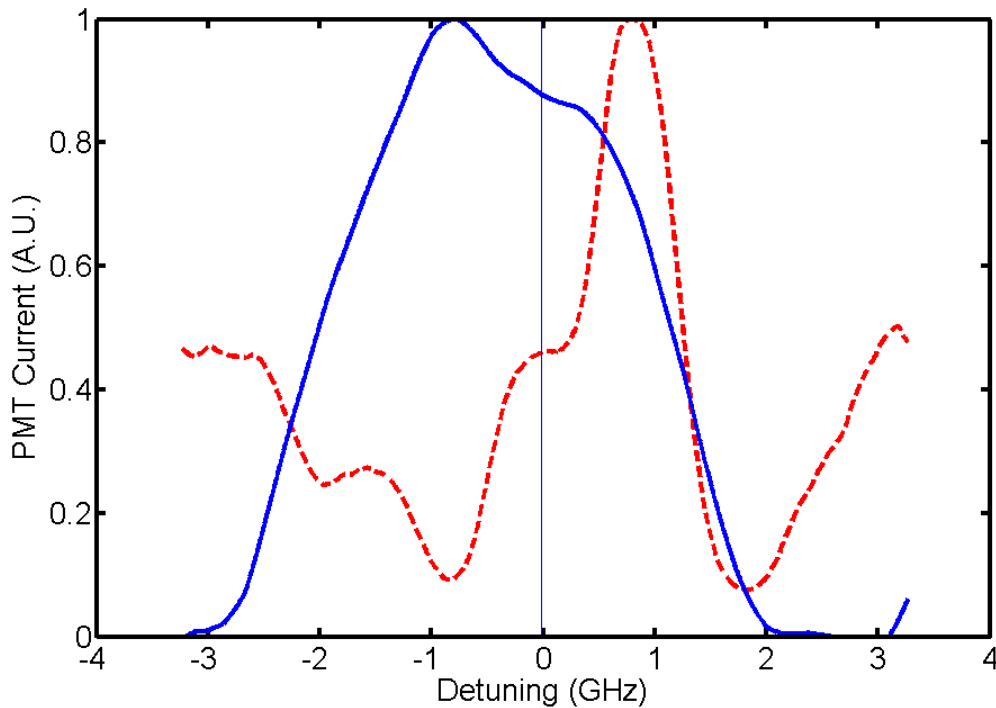

Fig. 20: Laser-induced fluorescence signal (solid blue) and iodine cell reference (dashed red) in an argon helicon plasma with 3.2 mTorr neutral pressure, 740 G magnetic field, and 390 W RF power.